Alachlor photocatalytic degradation over uncalcined Fe–TiO$_2$ loaded on granular activated carbon under UV and visible light irradiation

M.D.G. de Luna[a], K.K.P. Rivera[b,c], T. Suwannaruang[c,d], K. Wantala[c,d,e,*]

[a]Department of Chemical Engineering, University of the Philippines, 1101 Diliman, Quezon City, Philippines, Tel. +632 981 8500, ext. 3114; Fax: +632 929 6640; emails: mgdeluna@up.edu.ph, mgdeluna@ugmail.com (M.D.G. de Luna)
[b]Environmental Engineering Program, National Graduate School of Engineering, University of the Philippines, 1101 Diliman, Quezon City, Philippines, Tel. +632 981 8500, ext. 3114; email: kprivera@upd.edu.ph
[c]Chemical Kinetics and Applied Catalysis Laboratory (CKCL), Faculty of Engineering, Khon Kaen University, Khon Kaen 40002, Thailand, Tel. +664 336 2240; email: totsaporn.eng.kku@gmail.com (T. Suwannaruang), Tel./Fax: +664 336 2240, ext. 42; email: kitirote@kku.ac.th (K. Wantala)
[d]Faculty of Engineering, Department of Chemical Engineering, Khon Kaen University, Khon Kaen 40002, Thailand
[e]Faculty of Engineering, Research Center for Environmental and Hazardous Substance Management (EHSM), Khon Kaen University, Khon Kaen 40002, Thailand

Received 23 April 2014; Accepted 20 January 2015

ABSTRACT

Alachlor is a recalcitrant carcinogenic contaminant that may easily spread in water sources due to its wide usage as an herbicide. The aim of this study is to synthesize Fe–TiO$_2$ on granular activated carbon (GAC) support via hydrothermal method for the photocatalytic degradation of alachlor under ultraviolet and visible light irradiation. The effects of Fe–TiO$_2$ loading, initial alachlor concentration, and initial solution pH were determined using Box–Behnken design (BBD). X-ray diffraction (XRD) analysis of Fe–TiO$_2$-GAC samples showed anatase TiO$_2$ peaks as well as the graphite peak from carbon. Scanning electron microscope (SEM) images verified that Fe–TiO$_2$ was immobilized onto the GAC. In UV photocatalysis, the interaction between Fe and TiO$_2$ loading and initial alachlor concentration is significant wherein low Fe–TiO$_2$ loading and 50 ppm initial alachlor concentration increased the removal efficiency. In visible light photocatalysis, low Fe–TiO$_2$ loading and initial alachlor concentrations of 30 and 70 ppm are significant. The interactions of the initial solution pH with Fe–TiO$_2$ loading and initial alachlor concentration are also significant in which low solution pH increased alachlor removal for low Fe–TiO$_2$ loading and low initial concentration. The highest alachlor removal percentages obtained were 99.74 and 99.96% under UV and visible light irradiation, respectively. Total organic carbon analysis confirmed the mineralization of alachlor with 92.44 and 66.49% removal by UV and visible light photocatalysis, respectively.

Keywords: Alachlor; Box–Behnken design; Fe–TiO$_2$; Granular activated carbon support; Photocatalysis

*Corresponding author.

1. Introduction

Alachlor is a recalcitrant carcinogenic contaminant in drinking water monitored by the World Health Organization and the US Environmental Protection Agency [1]. Due to its wide usage as a primary herbicide for weed growth control, alachlor easily finds its way to the groundwater and other drinking water sources [1–3]. In the US, the maximum contaminant level for alachlor in drinking water is set at 0.002 mg/L, while its corresponding maximum residue level in Europe is 0.0001 mg/L [4].

Conventional methods are unable to remove alachlor completely from contaminated waters [4]. Various technologies have been applied for alachlor removal such as activated carbon [5,6], gamma radiolysis [7], hydrodynamic cavitation [8], ferrate oxidation [9], ozonation [10–13], photo-Fenton process [14], biological oxidation [14,15], sonochemical and ultrasonic treatments [16,17], and TiO_2 photocatalysis [18,19].

Titanium dioxide has been one of the most commonly used photocatalysts for the removal of organics in wastewater due to its strong oxidizing ability, nontoxicity, and photostability [18–23]. However, a typical problem common to TiO_2 photocatalysts is the fast recombination rate of the photogenerated electrons and holes, which leads to decreased photocatalytic activity [24]. In addition to this, the photocatalytic activity of pure TiO_2 is limited to UV irradiation because its energy band gap is at 3.2 eV. Metal doping with Fe^{3+} has been used to lower the bandgap and to extend the photoactivity of pure TiO_2 to the visible light spectrum [25,26]. The addition of Fe^{3+} to TiO_2 is very feasible since the small difference in their atomic radii enables the Fe ions to stably form a solid solution with TiO_2 [27]. Thus, Fe–TiO_2 photocatalysts tend to increase the photocatalytic activity of TiO_2 [28–30]. Ghorai et al. [29] demonstrated that Fe–doped TiO_2 was more photoactive in the removal of several organic dyes than P25 and commercial TiO_2 photocatalysts. Also, Tayade et al. [30] reported that the photocatalytic activity increased from 89 to 97% and from 57 to 83% for acetophenone and nitrobenzene removal in a 4 h of reaction time under bare TiO_2 and Fe–TiO_2, respectively.

Aside from the limitations by the high recombination rate and large energy band gap of TiO_2 photocatalysts, it also has issues when its powder form is used in aqueous systems. TiO_2 in powder form cannot be recycled because it cannot be separated from the solution readily [26]. The use of a support matrix such as granular activated carbon (GAC) will enable easy separation of the catalyst from the system and will also provide a larger surface area available as photocatalytic sites [31–34]. The support matrix enhances the light-gathering properties of the TiO_2 powder when it coats and adheres to its larger surface [35].

A combination of these two modification techniques will result in a composite of Fe–TiO_2 catalysts embedded on activated carbon, which has been investigated to determine the synergy of photocatalysis and adsorption [36,37]. Fe–TiO_2 photocatalysts supported on GAC showed higher photoactivity when compared to Fe–TiO_2 photocatalysts and TiO_2 on activated carbon combinations. This is due to the synergistic effects of the metal ion and the support matrix on TiO_2, including enhanced photoactivity under visible light and improved surface properties, respectively [36].

The preparations of Fe–TiO_2 photocatalysts on GAC support normally require calcination under a nitrogen atmosphere in order to activate the anatase TiO_2 crystalline phase and to remove impurities. However, in this study, the photocatalysts were synthesized by hydrothermal method without calcination. Photocatalytic degradation of alachlor was done in static reactors under UV and visible light. Box–Behnken design (BBD) generated using Minitab 16.0 (Minitab, Inc., Pennsylvania, USA) was used to investigate the effects of % Fe–TiO_2-GAC, initial alachlor concentration, and initial solution pH on alachlor removal under UV and visible light irradiation.

2. Materials and methods

2.1. Chemicals

Titanium tetrachloride ($TiCl_4$, 99%) from Merck Schuchardt OHG was used as the titanium dioxide catalyst precursor, 1,000 ppm Iron for atomic absorption standard as the dopant, and GAC (1,680–4,760 μm) purchased from Sigma-Aldrich as the support matrix. Synthetic alachlor PESTANAL analytical standard (99.2%), was dissolved in HPLC-grade distilled water from RCI Labscan Limited to prepare a 100 ppm stock solution. Hydrogen peroxide (H_2O_2, 30%) and ammonia solution (NH_4OH, 28%) were purchased from Ajax Finechem Pty Ltd., and QRёc, respectively. Isocratic-grade acetonitrile (CH_3CN, 99%) and methanol (CH_3OH, 99%) were purchased from Merck and RCI Labscan Limited, respectively.

2.2. Catalyst synthesis

Titanium dioxide doped with 0.20% wt Fe^{3+} (Fe–TiO_2) was prepared via hydrothermal method. $TiCl_4$ was dissolved in 400 mL cold deionized water and was stirred for 30 min. NH_4OH (90 mL) was introduced dropwise into the $TiCl_4$ solution. The resulting

white suspension was stirred for another 30 min in an ice bath, centrifuged, and decanted. The precipitates were washed with deionized water several times until the pH of the washing is neutral and then died at 40°C for 16 h to obtain amorphous TiO_2 powders.

Amorphous TiO_2 was dissolved in 30 mL H_2O_2. The solution was stirred for 30 min in an ice bath prior to dropwise addition of 90 mL H_2O_2. Doping was done by the addition of 0.84 mL 1,000 ppm Fe^{3+} solution. The solution was continuously stirred for 4 h until it became transparent yellow.

Meanwhile, GAC was soaked in 1.0 M HNO_3 for 24 h. Afterward, it was washed several times to remove excess acid and was dried at 100°C for 24 h. During the hydrothermal synthesis of the $Fe–TiO_2$-GAC catalysts, GAC was added to the $Fe–TiO_2$ solution after the 4 h stirring procedure. The following amounts of GAC were used: 5.4, 2.4, and 1.4 g for 10, 20, and 30% $Fe–TiO_2$-GAC, respectively. The resulting transparent yellow solution with GAC was transferred to a Teflon-lined steel autoclave and was subjected into hydrothermal treatment at 150°C for 8 h. The solution from the autoclave was filtered and dried as follows: (1) 40°C for 2 h, (2) 100°C for 4 h, and (3) 250°C for 4 h.

2.3. Analytical methods

X-ray diffraction analysis (XRD Model D8 Discover, Bruker AXS, Germany) was performed to confirm the presence of the crystalline anatase phase in the $Fe–TiO_2$ catalysts embedded on the GAC support. The obtained patterns were compared to those of $Fe–TiO_2$ and GAC. The following conditions were used: Cu Kα radiation at λ = 0.15406 nm, 40 kV potential, and 40 mA current. Scanning was done at a step of 0.02°/step from 2θ of 20° to 70°. Scanning electron microscopy (S-3000 N, Hitachi, Japan) was used to observe the morphologies of GAC and the GAC-supported catalysts at 500x magnification. The surface areas of the $Fe–TiO_2$-GAC photocatalysts were measured using Brunauer–Emmett–Teller analytical technique (NOVA 1200e, Quantachrome, USA).

Analysis of the remaining alachlor concentrations was done using high-pressure liquid chromatography (Waters e2695 HPLC, Harlow Scientific, USA) at the maximum absorption wavelength of 197 nm was used for the UV detector, with a mixture of 40% methanol and 60% acetonitrile as the mobile phase at a flow rate of 1.0 mL/min. Injection volume was 20 μL. The separation was performed by a Hypersil C18 ODS 4.0 mm × 125 mm 5 μm column. Total organic carbon (TOC) measurements were done using a TOC analyzer (multi N/C 2100S, Analytik Jena, Germany).

2.4. Photocatalytic degradation of alachlor

Static reactors were used in the photocatalytic degradation of alachlor with $Fe–TiO_2$-GAC catalysts. The effects of the amount of $Fe–TiO_2$ loaded on GAC, initial alachlor concentration, and initial solution pH were investigated following the experimental design in Table 1. $Fe–TiO_2$-GAC (1 g) catalysts was added to 10 mL alachlor solution, enough to fill a monolayer at the bottom of the static reactor. The durations of the photocatalytic degradation were 60 and 90 min for UV and visible light irradiation, respectively. The comparison of adsorption and photocatalysis under both UV and visible light irradiation was examined using pure GAC (1 g) and 20% $Fe–TiO_2$-GAC (1 g) catalyst and 10 mL of 50 ppm alachlor. Samples were filtered prior to chemical analysis.

3. Results and discussion

Alachlor removal percentages by the synthesized $Fe–TiO_2$-GAC photocatalysts under UV and visible light irradiation are summarized in Table 2. Under UV light irradiation (60 min), the highest alachlor removal (99.74%) was obtained using the following conditions: 10% $Fe–TiO_2$-GAC, 30 ppm initial alachlor concentration, and initial solution pH of 6. On the other hand, the highest alachlor removal (99.96%) under visible light irradiation was achieved at 10% $Fe–TiO_2$-GAC on alachlor solution with initial concentration of 50 ppm and initial solution pH of 4. The lowest removal percentages of 72.94 and 83.64% were attained for UV and visible light photocatalysis, respectively.

ANOVA statistics in Tables 3 and 4 shows that the RSM models for alachlor degradation under UV (R^2 = 0.9445) and visible light (R^2 = 0.9526) irradiation are both significant whereas the corresponding lack-of-fit errors are not significant. With UV irradiation (Table 3), none of the main effects are significant and only the interaction between $Fe–TiO_2$ loading and initial alachlor concentration is significant. With visible light (Table 4), the main effects of $Fe–TiO_2$ loading and initial alachlor concentration, as well as the interactions of initial solution pH with $Fe–TiO_2$ loading and initial alachlor concentration are significant.

The mathematical models for the photocatalytic degradation of alachlor under UV and visible light irradiation are given in Eqs. (1) and (2), respectively.

$$Y_1 = 77.57 - 1.60A + 0.07B - 0.39C + 9.45AB + 3.32AC + 1.81BC + 4.68A^2 + 7.91B^2 - 2.38C^2 \tag{1}$$

Table 1
Factors and levels for the photocatalytic degradation of alachlor

Factors	Symbol	Levels		
		−1	0	+1
% Fe–TiO$_2$ on GAC	A	10	20	30
Initial alachlor concentration (mg/L)	B	30	50	70
Initial solution pH	C	4	6	8

Table 2
Alachlor removal under UV and visible light using Fe–TiO$_2$-GAC

Run	% Fe–TiO$_2$ on GAC	Initial alachlor concetration (mg/L)	Initial solution pH	Alachlor removal (%)	
				UV (60 min)	VIS (90 min)
1	10	30	6	99.74	90.29
2	30	70	6	99.46	85.92
3	20	50	6	81.24	89.69
4	30	50	4	74.24	90.61
5	30	30	6	79.66	87.19
6	20	30	4	85.70	95.84
7	20	70	8	84.11	91.72
8	10	50	8	78.87	93.64
9	20	50	6	78.52	87.87
10	10	70	6	81.76	87.74
11	20	30	8	81.10	87.32
12	20	70	4	81.46	83.64
13	20	50	6	72.94	90.08
14	10	50	4	86.08	99.96
15	30	50	8	80.29	92.27

Table 3
ANOVA for alachlor removal under UV light with Fe–TiO$_2$-GAC

Source	df	Sum of squares	Mean square	F value	p-value	
Regression	9	768.221	85.358	9.46	0.012	Significant
Linear	3	21.733	7.244	0.80	0.544	
A—% Fe–TiO$_2$ on GAC	1	20.480	20.480	2.27	0.192	
B—Initial alachlor concn	1	0.044	0.044	0.00	0.947	
C—Initial solution pH	1	1.209	1.209	0.13	0.729	
Square	3	332.559	110.853	12.28	0.010	Significant
A^2	1	68.651	80.971	8.97	0.030	Significant
B^2	1	243.000	230.753	25.57	0.004	Significant
C^2	1	20.907	20.907	2.32	0.189	
Interaction	3	413.930	137.977	15.29	0.006	Significant
AB	1	356.832	356.832	39.53	0.001	Significant
AC	1	43.957	43.957	4.87	0.078	
BC	1	13.141	13.141	1.46	0.282	
Residual error	5	45.129	9.026			
Lack-of-fit	3	9.321	9.321	0.17	0.906	Not significant
Pure error	2	35.808	17.904			
Total	14	813.351				

Table 4
ANOVA for alachlor removal under visible light with Fe–TiO$_2$-GAC

Source	df	Sum of squares	Mean square	F value	p-value	
Regression	9	224.899	24.989	11.16	0.008	Significant
Linear	3	50.706	16.902	7.55	0.026	Significant
A—% Fe–TiO$_2$ on GAC	1	30.576	30.576	13.66	0.014	Significant
B—Initial alachlor concentration	1	16.878	16.878	7.54	0.041	Significant
C—Initial solution pH	1	3.251	3.251	1.45	0.282	
Square	3	88.974	29.658	13.25	0.008	Significant
A^2	1	8.412	8.653	3.86	0.106	
B^2	1	38.484	32.332	14.44	0.013	Significant
C^2	1	42.078	42.078	18.80	0.007	Significant
Interaction	3	85.220	85.220	12.69	0.009	Significant
AB	1	0.410	0.410	0.18	0.687	
AC	1	15.920	15.920	7.11	0.045	Significant
BC	1	68.890	68.890	30.77	0.003	Significant
Residual error	5	11.194	11.194			
Lack-of-fit	3	8.411	2.804	2.01	0.349	Not significant
Pure error	2	2.783	1.391			
Total	14	236.093				

$$Y_2 = 89.21 - 1.96A - 1.45B - 0.64C + 0.32AB + 2.00AC + 4.15BC + 1.53A^2 - 2.96B^2 + 3.38C^2$$

(2)

where Y_1 and Y_2 are the percentages of alachlor removal under UV and visible light irradiation, respectively; A is % Fe–TiO$_2$ on GAC, B is initial alachlor concentration, C is initial solution pH, AB is the interaction between % Fe–TiO$_2$ on GAC and initial alachlor concentration, AC is the interaction between % Fe–TiO$_2$ on GAC and initial solution pH, BC is the interaction between initial alachlor concentration and initial solution pH, and A^2, B^2, and C^2 are the quadratic terms for each of the main factors, respectively.

From Eqs. (1) and (2), the negative coefficients of Fe–TiO$_2$ loading indicate that the low amounts of Fe–TiO$_2$ results in high alachlor removals under UV and visible light irradiation. Under UV photocatalysis, the main effects are not significant and their coefficients have the lowest numerical values. The interaction between Fe-loading and initial alachlor concentration has a positive effect on alachlor removal and its contribution is the highest among all the factors as shown by its numerical coefficient. On the other hand, under visible light photocatalysis, all of the main effects have negative effects on alachlor removal. Of the three, the initial solution pH has the least impact on alachlor removal. The interactions between the initial solution pH with Fe loading and initial alachlor concentration are both significant and have more weight in the equation.

Based on BBD, the optimum conditions for alachlor degradation under UV and visible light irradiation are the same: 10% Fe–TiO$_2$ on GAC, initial alachlor concentration of 30 ppm, and initial solution pH of 4.

Fig. 1 compares the main effects of the factors on alachlor removal under the two different light sources. Increasing the Fe–TiO$_2$ loading on GAC decreases the alachlor removal. In both experimental setups (Table 2), the highest alachlor removal percentages are achieved at the lowest Fe–TiO$_2$ loading on GAC. From this, it can be inferred that adsorption by GAC plays a major role in alachlor removal. GAC is an effective adsorbent for alachlor removal [5,6]. The low amount of Fe–TiO$_2$ relative to the amount of GAC means that there are more adsorption sites than there are photocatalytic sites. Thus, it was possible that some of the alachlor have already been removed by adsorption onto the GAC before the photocatalysis with the Fe–TiO$_2$ occurred. For the catalysts containing 20 and 30% Fe–TiO$_2$-GAC, alachlor removal is not only predominantly ascribed to adsorption onto the GAC but also to the photocatalytic activity of Fe–TiO$_2$.

The main effect of the initial alachlor concentration on alachlor removal has opposite trends in UV and visible light photocatalysis. The initial alachlor concentration of 50 ppm has the lowest mean alachlor removal in UV photocatalysis while in visible light photocatalysis, it gave the highest mean alachlor removal. Opposing trends are also observed in the effect of initial solution pH on alachlor removal under UV and visible light irradiation. The initial solution pH of 6 gave the highest mean alachlor removal in
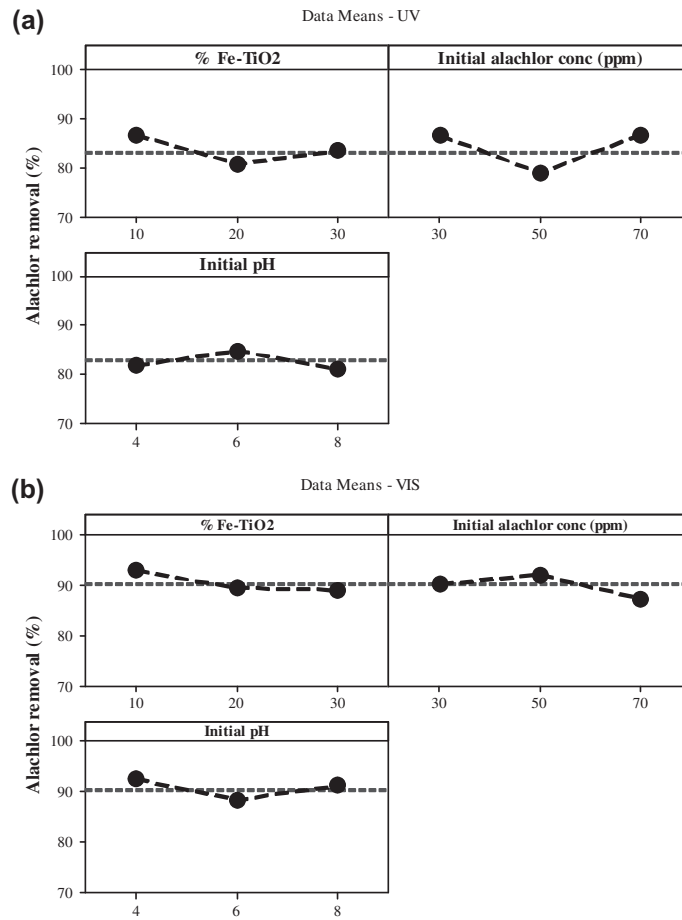
Fig. 1. Main effects for alachlor removal under UV light (a) and visible light (b) irradiations.
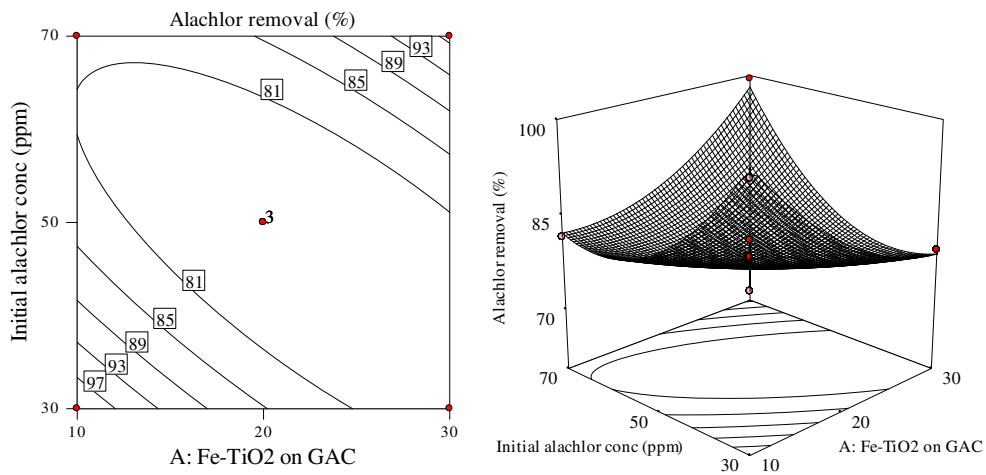

Fig. 2. Contour (a) and surface plots (b) for the interaction of Fe–TiO$_2$ loading on GAC and initial alachlor concentration on alachlor removal under UV light.
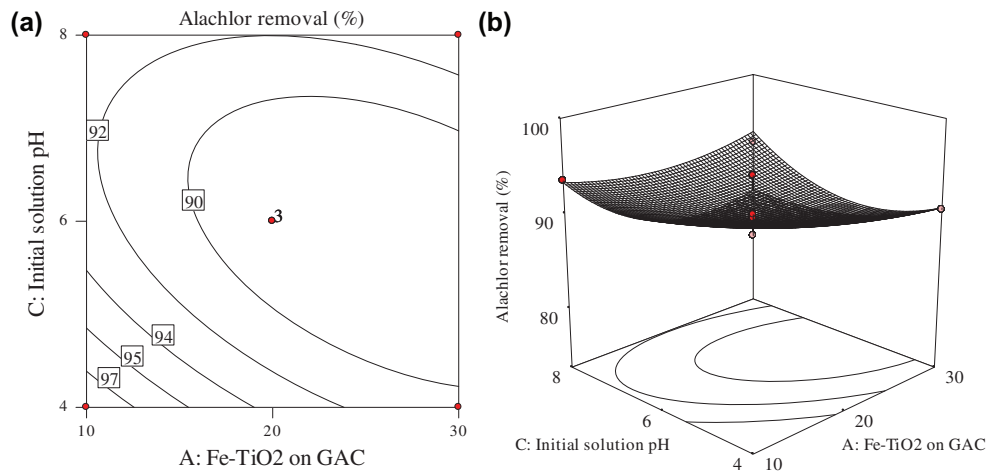
Fig. 3. Contour (a) and surface plots (b) for the interaction of Fe–TiO$_2$ loading on GAC and initial solution pH on alachlor removal under visible light.

UV photocatalysis while it gave the lowest mean alachlor removal in visible light photocatalysis.

In UV photocatalysis, the interaction of Fe–TiO$_2$ loading and initial alachlor concentration is significant (Fig. 2). It is observed that the combination of the extreme settings of both factors gives the highest alachlor removal percentages (Table 2). At 10% Fe–TiO$_2$ loading and 30 ppm initial alachlor concentration, alachlor removal was at 99.74%. At 30% Fe–TiO$_2$ loading and 70 ppm initial alachlor concentration, alachlor removal was at 99.46%.

On the other hand, the significant interactions in visible light photocatalysis are the interactions of initial solution pH with the Fe–TiO$_2$ loading on GAC and initial alachlor concentration, respectively.

Considering both pairs of interactions (Figs. 3 and 4), the highest alachlor removal percentages occur at the conditions with low initial solution pH (Table 2). At 10% Fe–TiO$_2$ loading and initial solution pH 4, alachlor removal was 99.96%. At 30 ppm initial alachlor concentration and initial solution pH 4, alachlor removal was at 95.84%. Although the main effect of initial solution pH alone is not significant in alachlor removal using Fe–TiO$_2$-GAC catalysts under visible light irradiation (Table 4), it has a considerable effect on both the catalyst and the alachlor in solution. The explanation for this is the point of zero charge of Fe–TiO$_2$ since GAC does not have a net charge in solution and is not sensitive to pH. At pH levels greater than 4, both the Fe–TiO$_2$ catalyst and alachlor
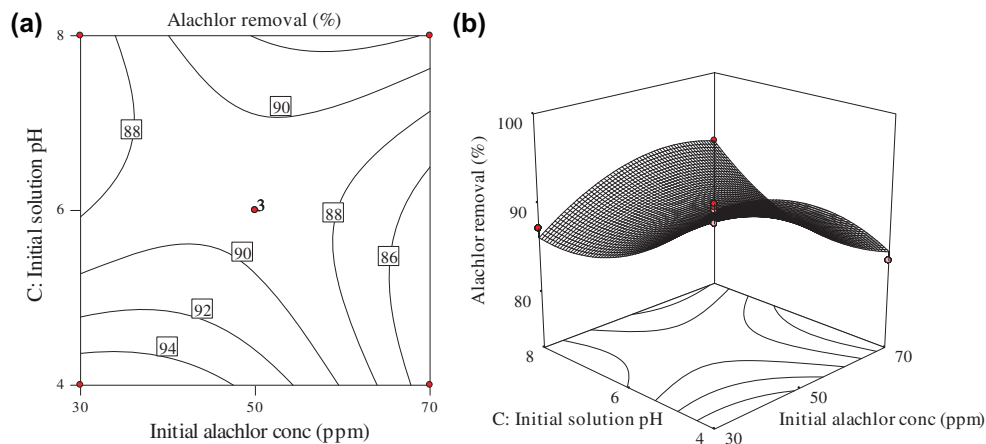

Fig. 4. Contour (a) and surface plots (b) for the interaction of initial alachlor concentration and initial solution pH on alachlor removal under visible light.
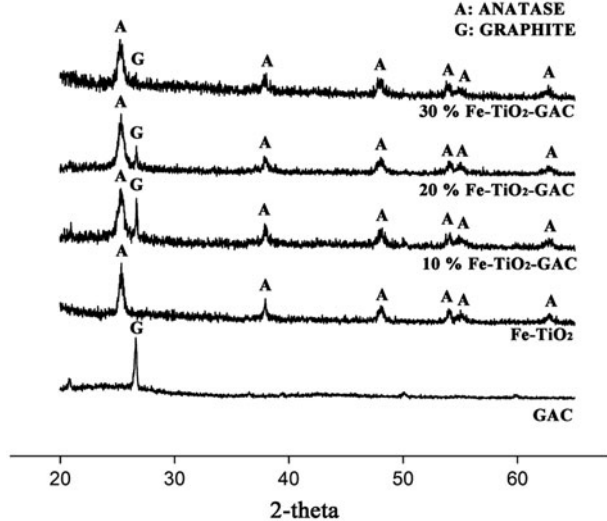
Fig. 5. XRD patterns of Fe–TiO$_2$-GAC, Fe–TiO$_2$, and GAC.

would exhibit negative charges [36]. This causes a slight repulsion between the two components resulting in decreased activity.

The XRD spectra of the Fe–TiO$_2$-GAC photocatalysts along with those of pure TiO$_2$ and pure GAC are shown in Fig. 5. All the major peaks of anatase TiO$_2$ at the 2θ positions of 25°, 38°, 48°, 55°, 56°, and 63° were present in the Fe–TiO$_2$-GAC photocatalysts [31,38–40]. The lone graphite peak at the 2θ position of 27° decreased with increasing amounts of Fe–TiO$_2$ loaded

onto GAC. No Fe peaks were detected since doping was done in a very small amount (0.20% wt. Fe).

Fig. 6 shows the Scanning electron microscope (SEM) images of the photocatalysts at 500× magnification. The surface of pure GAC (Fig. 6(a)) is rough, uneven, and porous. The incorporation of Fe–TiO$_2$ onto the GAC enhanced the smoothness of the catalyst surface. Moreover, as the amount of Fe–TiO$_2$ loading was increased from 10 to 30%, the degree of its coverage and dispersion on the GAC improved considerably.

BET surface area measurements of the Fe–TiO$_2$-GAC photocatalysts exhibited very large surface areas of 332.31, 465.43, and 423.96 m^2/g for 10, 20, and 30% Fe–TiO$_2$ on GAC, respectively. The surface area of pure GAC is about 506 ± 34 m^2/g [41]. The decrease in the surface area of GAC of about 45% for the 10% Fe–TiO$_2$-GAC catalyst can confirm the SEM results for the coating of Fe–TiO$_2$ on the surface of GAC. Thus, GAC is an effective support matrix for Fe–TiO$_2$ as it was able to increase the surface areas available for photocatalysis. Increasing the amount of Fe–TiO$_2$ loading from 10% to 20% enhanced the catalyst surface area by 40%. However, as the Fe–TiO$_2$ loading was increased from 20% to 30%, the surface area of the catalyst decreased slightly 9% due to the small amounts of GAC used in the catalyst preparation. The surface area of 20% Fe–TiO$_2$ loading was found to be the highest value compared to the other loading percentages. The lower loading amount of 10% Fe–TiO$_2$
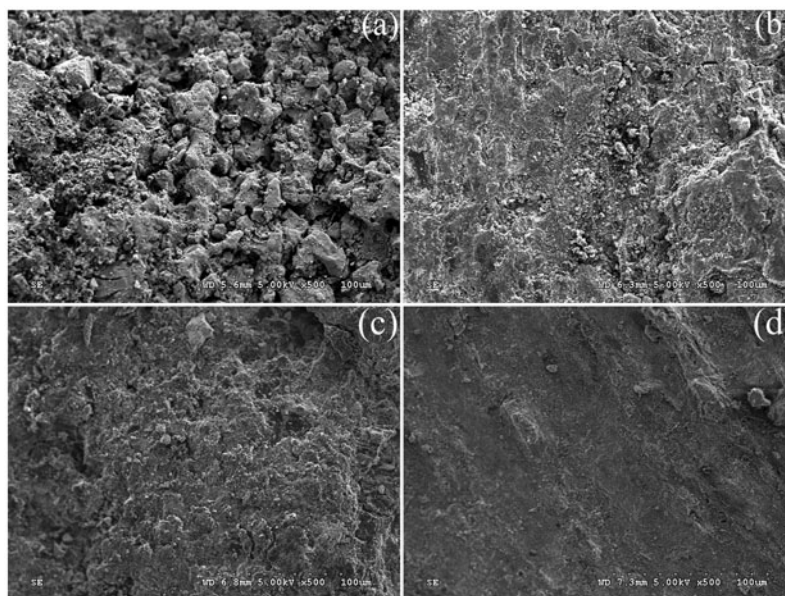

Fig. 6. SEM images of pure GAC (a) 10% (b) 20% (c) and 30% Fe–TiO$_2$ on GAC (d) at 500× magnification.
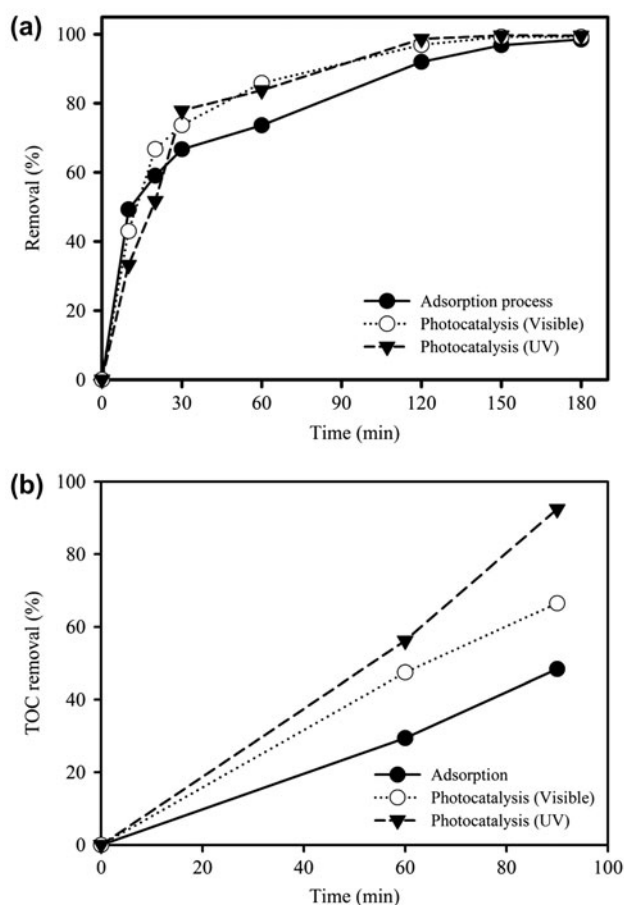
Fig. 7. (a) Alachlor and (b) TOC removal by adsorption and photocatalysis under UV and visible light irradiation. Initial alachlor concentration = 50 mg/L, 20% Fe–TiO$_2$-GAC dose = 1 g/10 mL, and pH = 6.0.

resulted in the insertion of the particles of the catalysts into the GAC pores, leading to a lower surface area. For the 20% Fe–TiO$_2$-GAC catalyst, the pseudo-pores of the powder catalysts seen in Fig. 6(c) enhanced the surface area. On the other hand, the surface area of the 30% Fe–TiO$_2$-GAC also has a lower value since these pseudo-pores were not present and that a smooth surface can be observed in Fig. 6(d).

The most significant observation in terms of the Fe–TiO$_2$ loading on the GAC can be explained through the physical characteristics of the catalysts. All catalysts have been able to significantly remove alachlor from the solution whether irradiation was provided by UV or visible light. Aside from the substantial increase in the BET surface areas, GAC was also able to act as an adsorbent, which enhanced alachlor removal.

Under both UV and visible light irradiation, the highest alachlor removal percentages of 99.74% and 99.96% were observed using 10% Fe–TiO$_2$-GAC. The catalyst with 10% Fe–TiO$_2$-GAC was chosen as an

optimum parameter in alachlor degradation. Thus, it can be said that for the catalysts with 10% Fe–TiO$_2$ on GAC, the mechanism of alachlor removal is mostly a combination of adsorption and photocatalysis. The same thing cannot be said with the catalyst with 30% Fe–TiO$_2$ on GAC. For this catalyst, there was a slight decrease in surface area due to the reduced amount of GAC added. Thus, the immediate action of adsorption has also slightly decreased. Since a corresponding decrease in photoactivity has not been observed, the catalyst was still able to effectively remove alachlor. The activity of the catalyst can then be attributed to photocatalysis than adsorption, as there is a greater amount of Fe–TiO$_2$ and lesser amount of GAC as compared to the other two catalysts.

In Fig. 7(a), it can be observed that both photocatalytic processes achieved 100% removal of the 50 ppm alachlor solution after 120 min of reaction, while it took adsorption 150 min. During the initial 20 min, adsorption is faster than photocatalysis. UV and visible light irradiation may not be sufficient to generate adequate quantities of electron and hole pairs. Tolosa et al. [37] also reported that adsorption occurs more readily than photocatalysis. However, from 30 min to 120 min, the photocatalytic experiments already showed faster degradation rates compared to adsorption. Eventhough adsorption plays a larger role in alachlor removal using Fe–TiO$_2$-GAC, the photocatalytic processes were still able to enhance the overall alachlor removal efficiency. In addition, the degradation rates of the photocatalytic processes under UV and visible light do not significantly differ past the 30 min point in the reaction. During the first 30 min, the removal under UV light irradiation is only slightly faster than under visible light irradiation.

Additionally, TOC removal was analyzed at 0, 60, and 90 min of reaction time and the results were displayed in Fig. 7(b). Results showed that TOC was found to be decreased in all processes, thus confirming the mineralization of alachlor. TOC removal by UV photocatalysis has the highest removal percentage at 92.44% followed by that for visible light photocatalysis at 66.49% and adsorption at 48.39%. Compared with alachlor removal, all processes demonstrated complete removal at 90 min of reaction time. Thus, the Fe–TiO$_2$-GAC photocatalysts may be used effectively in alachlor removal under both UV and visible light irradiation.

4. Conclusions

Fe–TiO$_2$ catalysts on GAC support can be synthesized via hydrothermal method without calcination. Photocatalytic degradation of alachlor was carried out

using static reactors under UV and visible light irradiation. Under UV light irradiation, alachlor removal ranged from 72.94 to 99.74%, whereas it ranged from 83.64 to 99.96% under visible light irradiation. ANOVA determined that both regression models for photocatalysis under UV and visible light irradiation are significant with R^2 values of 0.9445 and 0.9526, respectively. BBD determined that only the interaction effect between of Fe–TiO_2 loading on GAC and initial alachlor concentration and their respective quadratic effects are significant in UV photocatalysis. On the other hand, under visible light photocatalysis, the significant factors are the main effects of Fe–TiO_2 loading and initial alachlor concentration, the interaction effects of initial solution pH with Fe–TiO_2 loading and initial alachlor concentration, and the quadratic effects of the initial alachlor concentration and initial solution pH. The optimum conditions for alachlor photocatalytic degradation under UV and visible light irradiation are 10% Fe–TiO_2 loading on GAC, 30 ppm initial alachlor concentration, and initial solution pH of 4.

Acknowledgments

References

[1] S. Galassi, A. Provini, S. Mangiapan, E. Benfenati, Alachlor and its metabolites in surface water, Chemosphere 32(2) (1996) 229–237.

[2] A. Ramesh, S.T. Maheswari, Dissipation of alachlor in cotton plant, soil, and water and its bioaccumulation in fish, Chemosphere 54 (2004) 647–652.

[3] C.W. Knapp, D.W. Graham, G. Berardesco, F. de Noyelles Jr., B.J. Cutak, C.K. Larive, Nutrient level, microbial activity, and alachlor transformation in aerobic aquatic systems, Water Res. 37(19) (2003) 4761–4769.

[4] J.A. Gabaldon, J.M. Cascales, A. Maquieira, R. Puchades, Rapid trace analysis of alachlor in water and vegetable samples, J. Chromatogr. A 963 (2002) 125–136.

[5] S. Baup, C. Jaffre, D. Wolbert, A. Laplanche, Adsorption of pesticides onto granular activated carbon: Determination of surface diffusivities using simple batch experiments, Adsorption 6 (2000) 219–228.

[6] B.N. Badriyha, V. Ravindran, W. Den, M. Pirbazari, Bioadsorber efficiency, design and performance forecasting for alachlor removal, Water Res. 37 (2003) 4051–4072.

[7] D. Choi, O.M. Lee, S. Yu, S.W. Jeong, Gamma radiolysis of alachlor aqueous solutions in the presence of hydrogen peroxide, J. Hazard. Mater. 184 (2010) 308–312.

[8] X. Wang, Y. Zhang, Degradation of alachlor in aqueous solution by using hydrodynamic cavitation, J. Hazard. Mater. 161 (2009) 202–207.

[9] J.H. Zhu, X.L. Yan, Y. Liu, B. Zhang, Improving alachlor biodegradability by ferrate oxidation, J. Hazard. Mater. B135 (2006) 94–99.

[10] H. Li, J.H. Qu, H.J. Liu, Decomposition of alachlor by ozonation and its mechanism, J. Environ. Sci. 19 (2007) 769–775.

[11] Z. Qiang, C. Liu, B. Dong, Y. Zhang, Degradation mechanism of alachlor during direct ozonation and O_3/H_2O_2 advanced oxidation process, Chemosphere 78 (2010) 517–526.

[12] J. Qu, H. Li, H. Liu, H. He, Ozonation of alachlor by Cu/Al_2O_3 in water, Catal. Today 90 (2004) 291–296.

[13] F. Beltran, B. Acedo, J. Rivas, Use of ozone and hydrogen peroxide to remove alachlor from surface water, J. Environ. Contam. Toxicol. 63 (1999) 9–14.

[14] M.M. Ballesteros Martin, J.A. Sanchez Perez, J.L. Garcia Sanchez, L. Montes de Oca, J.L. Casas Lopez, I. Oller, S. Malato Rodriguez, Degradation of alachlor and pyrimetharil by combined photo-Fenton and biological oxidation, J. Hazard. Mater. 155 (2008) 342–349.

[15] M. Slaba, R. Szewczyk, M.A. Piatek, J. Dlogonski, Alachlor oxidation by the filamentous fungus *Paecilomyces marquandii*, J. Hazard. Mater. 261 (2013) 443–450.

[16] M.V. Bagal, P.R. Gogate, Sonochemical degradation of alachlor in the presence of process intensifying additives, Sep. Purif. Technol. 90 (2012) 92–100.

[17] R.A. Torres, R. Mosteo, C. Petrier, C. Pulgarin, Experimental design approach to the optimization of ultrasonic degradation of alachlor and enhancement of treated water biodegradability, Ultrason. Sonochem. 16 (2009) 425–430.

[18] C.C. Wong, W. Chu, The direct photolysis and photocatalytic degradation of alachlor at different TiO_2 and UV sources, Chemosphere 50 (2003) 981–987.

[19] Y. Xin, H. Liu, L. Han, Y. Zhou, Comparative study of photocatalytic and photoelectrocatalytic properties of alachlor using different morphology of TiO_2/Ti photoelectrodes, J. Hazard. Mater. 192 (2011) 1812–1818.

[20] C.L. Bahena, S.S. Martinez, Photodegradation of chlorbromuron, atrazine, and alachlor in aqueous systems under solar irradiation, Int. J. Photoenergy 2006 (2006) 1–6.

[21] W. Chu, C.C. Wong, Study of herbicide alachlor removal in a photocatalytic process through the examination of the reaction mechanism, Ind. Eng. Chem. Res. 43 (2004) 5027–5031.

[22] C.C. Wong, W. Chu, The hydrogen peroxide-assisted photocatalytic degradation of alachlor in TiO_2 suspensions, Environ. Sci. Technol. 37 (2003) 2310–2316.

[23] S. Yao, J. Li, Z. Shi, Immobilization of TiO_2 nanoparticles on activated carbon fiber and its photodegradation performance for organic pollutants, Particuology 8 (2010) 272–278.

[24] C.A. Castro-Lopez, A. Centeno, S.A. Giraldo, Fe-modified TiO2 photocatalysts for the oxidative degradation of recalcitrant water contaminants, Catal. Today 157 (2010) 119–124.

[25] K. Wantala, L. Laokiat, P. Khemthong, N. Grisdanurak, K. Fukaya, Calcination temperature effect on solvothermal Fe-TiO_2 and its performance under visible light irradiation, J. Taiwan Inst. Chem. E 41 (2010) 612–616.

[26] X. Wang, Y. Tang, M.Y. Leiw, T.T. Lim, Solvothermal synthesis of Fe-C co-doped TiO_2 nanoparticles for visible-light photocatalytic removal of emerging organic contaminants in water, Appl. Catal. A: Gen. 409–410 (2011) 257–266.

[27] N.A. Jamalludin, A.Z. Abdullah, Reactive dye degradation by combined Fe(III)/TiO_2 catalyst and ultrasonic irradiation: Effect of Fe(III) loading and calcination temperature, Ultrason. Sonochem. 18 (2011) 669–678.

[28] S. Liu, Y. Chen, Enhanced photocatalytic activity of TiO2 powders doped by Fe unevenly, Catal. Commun. 10 (2009) 894–899.

[29] T.K. Ghorai, S.K. Biswas, P. Pramanik, Photooxidation of different organic dyes (RB, MO, TB, and BG) using Fe(III)-doped TiO_2 nanophotocatalyst prepared by novel chemical method, Appl. Surf. Sci. 254 (2008) 7498–7504.

[30] R.J. Tayade, R.G. Kulkarni, R.V. Jasra, Transition metal ion impregnated mesoporous TiO_2 for photocatalytic degradation of organic contaminants in water, Ind. Eng. Chem. Res. 45 (2006) 5231–5238.

[31] M. Asiltürk, S. Sener, TiO_2-activated carbon photocatalysts: Preparation, characterization and photocatalytic activities, Chem. Eng. J. 180 (2012) 354–363.

[32] S.M. Lam, J.C. Sin, A.R. Mohamed, Parameter effect on photocatalytic degradation of phenol using TiO_2-P25/activated carbon (AC), Korean J. Chem. Eng. 27 (2010) 1109–1116.

[33] S.M. Lam, J.C. Sin, A.R. Mohamed, Optimizing photocatalytic degradation of phenol by TiO_2/GAC using response surface methodology, Korean J. Chem. Eng. 28 (2011) 84–92.

[34] C.Y. Kuo, C.H. Wu, S.T. Chen, Decolorization of C.I. Reactive Red 2 by UV/TiO_2/PAC and visible light/TiO_2/PAC systems, Desalin. Water Treat. 52 (2014) 834–843.

[35] S. Yao, J. Li, Z. Shi, Immobilization of TiO_2 nanoparticles on activated carbon fiber and its photodegradation performance for organic pollutants, Particuology 8 (2010) 272–278.

[36] Y. Li, J. Chen, J. Liu, M. Ma, W. Chen, L. Li, Activated carbon supported TiO_2-photocatalysts doped with Fe ions for continuous treatment of dye wastewater in a dynamic reactor, J. Environ. Sci. 22 (2010) 1290–1296.

[37] N.C. Tolosa, M.C. Lu, H.D. Mendoza, A.P. Rollon, The effect of the composition of tri-elemental doping (K, Al, S) on the photocatalytic performance of synthesized TiO_2 nanoparticles in oxidizing 2-chlorophenol over visible light illumination, Appl. Catal. A: Gen. 401 (2011) 233–238.

[38] K. Wantala, S. Neramittagapong, A. Neramittagapong, K. Kasipar, S. Khaownetr, S. Chuichucherm, Photocatalytic degradation of alachlor on Fe-TiO_2-immobilized on GAC under black light irradiation using Box–Behnken design, Mater. Sci. Forum 734 (2013) 306–316.

[39] K. Wantala, P. Khemthong, J. Wittayakun, N. Grisdanurak, Visible light-irradiated degradation of alachlor on Fe-TiO_2 with assistance of H_2O_2, Korean J. Chem. Eng. 28(11) (2011) 2178–2183.

[40] H. Slimen, A. Houas, J.P. Nogier, Elaboration of stable anatase TiO_2 through activated carbon addition with high photocatalytic activity under visible light, J. Photochem. Photobiol. A: Chem. 221 (2011) 13–21.

[41] J.R. Kastner, J. Miller, K.C. Das, Pyrolysis conditions and ozone oxidation effects on ammonia adsorption in biomass generated chars, J. Hazard. Mater. 164(2–3) (2009) 1420–1427.